Report

Cell Reports

KMT2A and KMT2B Mediate Memory Function by Affecting Distinct Genomic Regions

Graphical Abstract

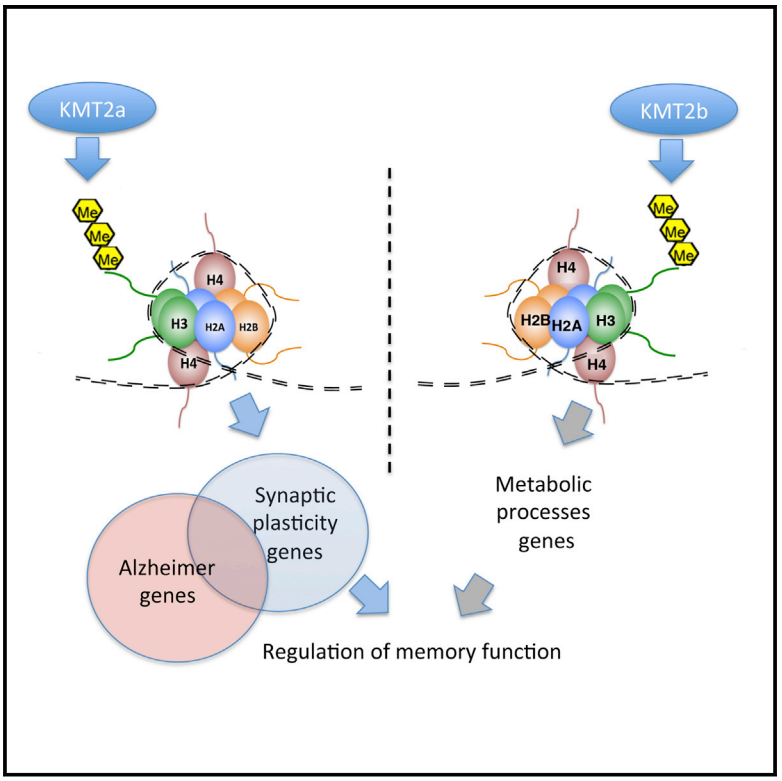

Authors

Cemil Kerimoglu, M. Sadman Sakib, Gaurav Jain, ..., Andrea Kranz, A. Francis Stewart, Andre Fischer

Correspondence

andre.fischer@dzne.de

In Brief

Kerimoglu et al. report that the related histone methyltransferases Kmt2a and Kmt2b are both required for memory function but control different neuronal gene-expression programs. Loss of Kmt2a partially recapitulates changes in H3K4me3 seen in Alzheimer's models.

Highlights

- The related histone methyltransferases Kmt2a and Kmt2b regulate memory function
- Loss of Kmt2a or Kmt2b impacts H3K4 methylation at distinct genomic regions
- Neuronal Kmt2a and Kmt2b affect distinct gene-expression programs
- Loss of Kmt2a partially reflects changes observed in a model for Alzheimer's disease

Accession Numbers

GSE99250

Kerimoglu et al., 2017, Cell Reports *20*, 538–548
July 18, 2017
http://dx.doi.org/10.1016/j.celrep.2017.06.072

OPEN ACCESS
CellPress

Cell Reports
Report

KMT2A and KMT2B Mediate Memory Function by Affecting Distinct Genomic Regions

Cemil Kerimoglu,[1] M. Sadman Sakib,[2] Gaurav Jain,[2] Eva Benito,[2] Susanne Burkhardt,[2] Vincenzo Capece,[2] Lalit Kaurani,[2] Rashi Halder,[2,4] Roberto Carlos Agís-Balboa,[2,5] Roman Stilling,[2,6] Hendrik Urbanke,[2] Andrea Kranz,[3] A. Francis Stewart,[3] and Andre Fischer[1,2,7,*]

[1]Department for Psychiatry and Psychotherapy, University Medical Center Goettingen, Goettingen 37075, Germany
[2]German Center for Neurodegenerative Diseases, Epigenetics, and Systems Medicine in Neurodegenerative Diseases, University Medical Center Goettingen, Goettingen 37075, Germany
[3]Biotechnology Center, Dresden University of Technology, Dresden 01069, Germany
[4]Present address: Luxembourg Centre for Systems Biomedicine, University of Luxembourg, Esch-sur-Alzette 4365, Luxembourg
[5]Present address: Psychiatric Diseases Research Group, Galicia Sur Health Research Institute, Complexo Hospitalario Universitario de Vigo (CHUVI), SERGAS, CIBERSAM, Vigo 36201, Spain
[6]Present address: German Primate Center, Goettingen 37075, Germany
[7]Lead Contact
*Correspondence: andre.fischer@dzne.de
http://dx.doi.org/10.1016/j.celrep.2017.06.072

SUMMARY

Kmt2a and Kmt2b are H3K4 methyltransferases of the Set1/Trithorax class. We have recently shown the importance of Kmt2b for learning and memory. Here, we report that Kmt2a is also important in memory formation. We compare the decrease in H3K4 methylation and de-regulation of gene expression in hippocampal neurons of mice with knockdown of either Kmt2a or Kmt2b. Kmt2a and Kmt2b control largely distinct genomic regions and different molecular pathways linked to neuronal plasticity. Finally, we show that the decrease in H3K4 methylation resulting from Kmt2a knockdown partially recapitulates the pattern previously reported in CK-p25 mice, a model for neurodegeneration and memory impairment. Our findings point to the distinct functions of even closely related histone-modifying enzymes and provide essential insight for the development of more efficient and specific epigenetic therapies against brain diseases.

INTRODUCTION

Regulation of posttranslational histone modifications has been implicated in memory formation, and its de-regulation is linked to cognitive disorders (Day and Sweatt, 2011; Jakovcevski and Akbarian, 2012; Fischer, 2014). Histone methylation is controlled by the opposing activity of lysine methyltransferases (KMTs) and lysine demethylases (KDMs). Unlike histone acetylation, lysine residues of histones can be mono-, di-, or trimethylated. Histone 3 lysine 4 trimethylation (H3K4me3) is enriched around transcription start site (TSS) regions of actively transcribed and/or poised genes (Guenther et al., 2005), whereas histone 3 lysine 4 monomethylation (H3K4me1) is enriched at enhancers (Heintzman et al., 2009). H3K4 methylation is mediated by SET proteins. Set1 is the only H3K4 KMT in yeast (Roguev et al., 2001). *Drosophila* encodes three different SET proteins—Set1, trithorax (trx), and trithorax-related (trr) (Mohan et al., 2011)—whereas mammals possess six SET-related H3K4 methyltransferases—Kmt2a (Mll1), Kmt2b (Mll2), Kmt2c (Mll3), Kmt2d (Mll4), Setd1a, and Setd1b. Kmt2a/Kmt2b are related to trx, Kmt2c/Kmt2d to trr, and Setd1a/Setd1b to Set1 (Shilatifard, 2012). The existence of several homologous histone-modifying enzymes mediating the same modifications raises the question of redundancy versus specificity of their actions. This is especially true for brain regions such as the hippocampus, which is intimately linked to memory function, where all six H3K4 KMTs are strongly expressed (see, for example, hippocampal RNA sequencing [RNA-seq] data published in Benito et al., 2015 or RNA-seq data from wild-type mice reported in this study).

The specific roles of H3K4 KMTs in neurons and memory function have not been investigated systematically so far. In this study, we begin to address this issue by comparing the roles of Kmt2a and Kmt2b. We measure H3K4me3/me1 patterns and related gene expression specifically in hippocampal neurons of mice lacking Kmt2a (Kmt2a cKO) or Kmt2b (Kmt2b cKO) in excitatory forebrain neurons of the adult brain. Both cKO mice display impaired memory consolidation (Kerimoglu et al., 2013; this study). Moreover, we find that the two KMTs regulate genomic regions associated with unique cellular functions.

RESULTS

Kmt2a cKO Mice Exhibit Impaired Hippocampus-Dependent Memory Formation

We have previously shown that Kmt2b cKO mice have memory impairment (Kerimoglu et al., 2013). Here, we generated Kmt2a cKO mice using the same Cre/loxP strategy (Kerimoglu et al., 2013; Minichiello et al., 1999) to ensure deletion of Kmt2a in adult excitatory forebrain neurons and confirmed its knockdown in hippocampus (Figures S1A–S1C). We then subjected Kmt2a cKO and control littermates to behavioral testing. There was no difference in time spent in center of the open field among groups (Figure S1D; $p = 0.37$). Kmt2a cKO mice, however, spent more

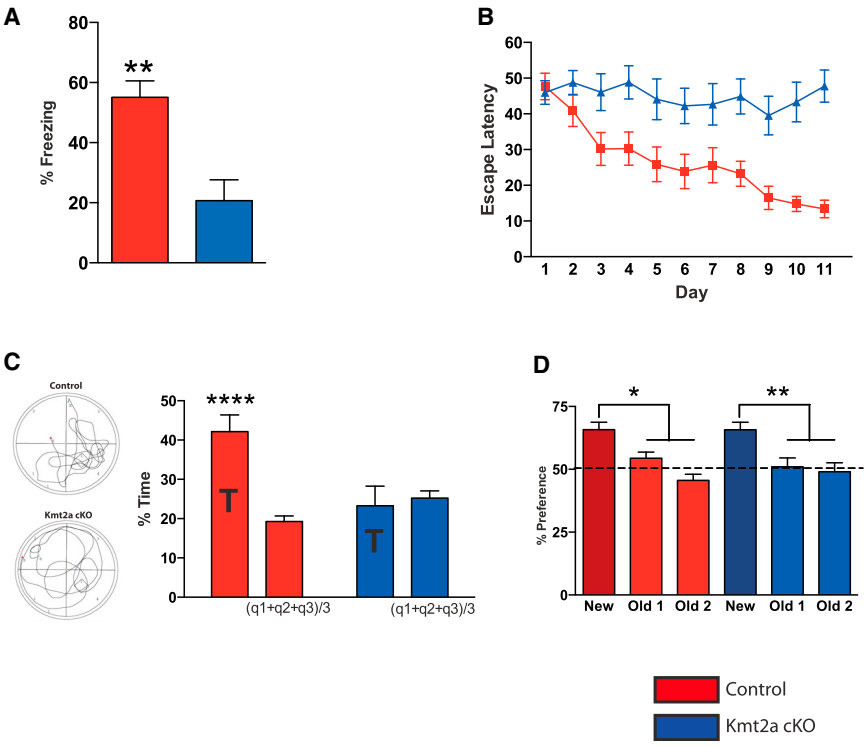

Figure 1. Kmt2a Is Required for Memory Consolidation

(A) Kmt2a cKO mice show significantly lower freezing compared to controls in context-dependent fear-conditioning test (**$p < 0.01$; control n = 12, Kmt2a cKO n = 9).

(B) Kmt2a cKO mice fail to acquire the memory of the location of a hidden platform in water maze test (two-way ANOVA genotype effect $p < 0.001$; control n = 14; Kmt2a cKO n = 13).

(C) (Left) Representative swim path during probe test. (Right) Control mice show a significant preference to target quadrant (****$p < 0.001$), whereas Kmt2a cKO mice do not (control n = 14; Kmt2a cKO n = 13).

(D) Kmt2a cKO (n = 17) and their control littermates (n = 19) explored both objects ("old1" and "old2") similarly during 5 min training. 24 hr later, both of them showed a significant preference to the novel object ("new"; **$p < 0.01$; *$p < 0.05$).

time in the open arms of elevated plus maze, indicating anxiolytic behavior (Figure S1E; $p < 0.001$). No difference was observed for depressive-like behavior (Figure S1F; $p = 0.67$). Kmt2a cKO mice displayed impaired associative memory in the fear-conditioning paradigm (Figure 1A; $p < 0.01$) and impaired spatial memory in water maze test (Figure 1B: escape latency two-way ANOVA genotype effect: $p < 0.001$; Figure 1C: probe test, preference to the target quadrant: $p = 0.7$ for Kmt2a cKO, $p < 0.0001$ for control). Swim speed was similar among groups (Figure S1G; $p = 0.39$). Differently from Kmt2b cKO (Kerimoglu et al., 2013), object recognition memory was not affected in Kmt2a cKO mice (Figure 1D).

Loss of Kmt2a and Kmt2b Affects H3K4me3 at Unique Genomic Regions

We performed chromatin immunoprecipitation sequencing (ChIP-seq) on neuronal nuclei sorted by fluorescence-activated cell sorting (FACS) (Benito et al., 2015; Halder et al., 2016) from hippocampal CA region of Kmt2a cKO and Kmt2b cKO mice and their control littermates. In both cKO mice, the amount of neurons obtained after cell sorting was similar to their respective controls, confirming that loss of Kmt2a or Kmt2b does not cause neurodegeneration (Figures S2A and S2B). Knockdown of Kmt2a or Kmt2b leads to a significant decrease in H3K4me3, which is especially obvious at transcription start sites (TSSs) (Figures 2A and 2B), without affecting bulk H3K4me3 in CA tissue (Figures S2C and S2D). We detected 4,964 genes with decreased and only four genes with increased H3K4me3 at TSS regions in Kmt2a cKO neurons (Figure 2C, upper panel). In contrast, in Kmt2b cKO, there were 2,801 genes with decreased and 112 genes with increased H3K4me3 at TSS regions (Figure 2C, upper panel). We cannot exclude that part of the observed changes are due to secondary effects, but the finding that the vast majority of the observed changes reflect decreased H3K4me3 is in line with the loss of H3K4-methyltransferase activity. Interestingly, the genes showing decreased H3K4me3 at the TSS in Kmt2a cKO and Kmt2b cKO differ substantially (Figure 2C, lower panel) and represent different functional categories (Figures 2D and 2E). Genes affected by loss of Kmt2a are involved in transcriptional regulation, chromatin binding, mRNA processing, and protein ubiquitination (Figures 2D, 2F, and S3A), whereas those in Kmt2b cKO are broadly involved in neuronal protrusion-related categories—i.e., Wnt signaling, cytokine and growth factor activity, matrix metalloprotease activity, cell adhesion, and angiogenesis (Figures 2E, 2F, and S3B).

TSS regions with decreased H3K4me3 in Kmt2a cKO mice are specifically enriched (E value < 0.05) for the consensus sequence (CGGAAGTG) representing 26 transformation-specific (ETS) transcription factors (Figure 2G; Data S1), whereas those in Kmt2b cKO are enriched for a sequence specific for E2F transcription factors (GGCGGGA; Figure 2G; Data S1).

The decrease in TSS-associated H3K4me3 is more widespread but less severe in Kmt2a cKO than in Kmt2b cKO. With false discovery rate (FDR) < 0.1 and fold change > 1.2, there are 5,182 TSS regions with decreased H3K4me3 in Kmt2a cKO in contrast to 2,963 in Kmt2b cKO (Figure 2H). There are, however, far less TSS regions in Kmt2a cKO than in Kmt2b cKO, at which H3K4me3 is decreased more than 2-fold (Figure 2H)—i.e., 267 in Kmt2a cKO versus 2,314 in Kmt2b cKO using FDR < 0.1.

Knockdown of Kmt2a or Kmt2b Leads to De-regulation of Unique Gene-Expression Programs

By RNA sequencing, we observed 471 genes down- and 225 genes upregulated in Kmt2a cKO (Figure 3A) and 485 genes

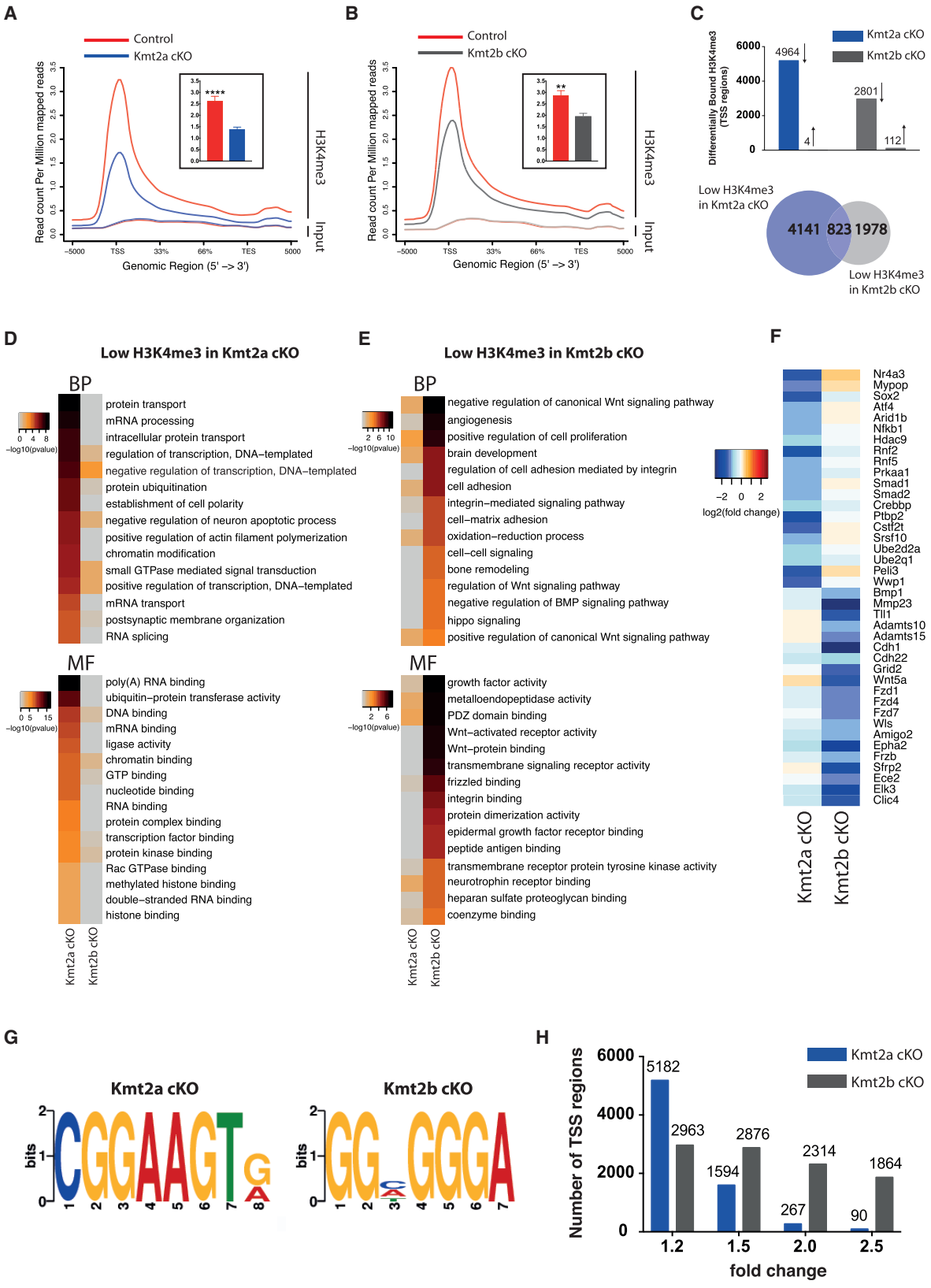

(legend on next page)

down- versus 89 genes upregulated in Kmt2b cKO mice in comparison to controls (Figure 3B). There was again little overlap between genes affected in Kmt2a cKO and Kmt2b cKO mice (Figure 3C). In both cKO mice, there was a significant overlap between decreased gene expression and decreased H3K4me3 at TSS (Figure 3D; hypergeometric test: $p < 0.0001$). With a lower threshold for differential H3K4me3 binding, there was an even greater overlap (Figures S4A and S4B). Genes that were previously shown to be downregulated and have decreased H3K4me3 at their promoters in Kmt2b cKO (Kerimoglu et al., 2013) and those observed in this study in Kmt2a cKO mice were confirmed in our RNA-seq/ChIP-seq and qPCR/ChIP-qPCR analyses, respectively (Figures S5A–S5D). Loss of Kmt2a or Kmt2b did not impact H3 turnover (Figures S5E and S5F).

Genes showing concomitant downregulation and decrease in H3K4me3 in Kmt2a cKO are involved in neuronal and synaptic development (Figure 3E), whereas those in Kmt2b cKO group into metabolism-related processes (Figure 3F).

In both cKO mice, a large number of genes exhibit decreased H3K4me3, whereas their expression is not affected (Figure 3D). This was particularly true for stimulus-inducible immediate early genes (IEGs) (Figures 3G and 3H) in Kmt2a cKO mice and is in line with findings that H3K4me3 does not always relate to transcriptional activity and can be a mark for "primed" genes (Andreu-Vieyra et al., 2010; Denissov et al., 2014; Guenther et al., 2005; Wang et al., 2009).

Loss of Kmt2a and Kmt2b Affects H3K4 Monomethylation at Unique Genomic Regions

Similar to H3K4me3, we observed a substantial decrease in the levels of H3K4me1, an established enhancer mark (Heintzman et al., 2009), in hippocampal Kmt2a cKO neurons (Figure 4A; 8,863 regions decreased and 914 regions increased with FDR < 0.1 and fold change > 1.2). The effect in Kmt2b cKO neurons was comparatively modest (Figure 4A; 1,154 regions decreased and 324 regions increased with FDR < 0.1 and fold change > 1.2). Again, there was little overlap in the genomic regions that exhibited decreased H3K4me1 in Kmt2a cKO and Kmt2b cKO mice (Figure 4B). Interestingly, each of these enzymes mediates H3K4 mono- and trimethylation independently at non-overlapping genomic locations (Figures 4C and 4D).

Given that H3K4me1 is enriched at enhancers, we also explored long-distance interactions linked to regions with decreased H3K4me1, using information about topological association domains (TADs) available for mouse cortex (Dixon et al., 2012). We identified gene promoters located in 40-kb TAD bins interacting with those possessing significantly decreased H3K4me1 peaks, filtered them further keeping only the regions with interaction scores beyond 1 SD from the mean (Figure 4E) and subjected the final list to functional Gene Ontology (GO) analysis. In Kmt2a cKO, we observed enrichment in categories related to transcriptional regulation and neuronal signaling (Figures 4F–4H; Data S2). There was no clear category enrichment in Kmt2b cKO (Data S2). Moreover, decreased H3K4me1 at TSS did not significantly overlap with decreased gene expression (Figures S4C and S4D). Finally, gene promoters interacting with decreased H3K4me1 peaks do not significantly overlap with those having decreased H3K4me3 in Kmt2a cKO neurons (Figure 4I).

Comparison of H3K4me3 in Kmt2a and Kmt2b cKO Mice to H3K4 Changes Observed in a Mouse Model for Neurodegeneration

We compared the changes in H3K4me3 detected in our cKO mice to a previously published dataset obtained from the hippocampus of CK-p25 mice, a mouse model of Alzheimer's disease (Gjoneska et al., 2015). Six weeks of p25 induction results in decreased H3K4me3 at the promoters of memory-related genes (Gjoneska et al., 2015). We remapped and reanalyzed those datasets (GEO: GSE65159) using our parameters (see Experimental Procedures) and confirmed that genes with reduced H3K4me3 in CK-p25 mice are involved in synaptic plasticity (Figure S6). Interestingly, 52% of the genes with decreased H3K4me3 at TSS regions in CK-p25 mice showed also decreased H3K4me3 in Kmt2a cKO mice (Figure 5A). Although the number of genes showing decreased H3K4me3 was five times higher in Kmt2a cKO mice (using the exact same FDR and log2 fold change cutoff), the overlap between both gene sets is significant (hypergeometic test $p < 0.0001$). Using the same approach to compare the genes linked to reduced H3K4me3 in CK-p25 and Kmt2b mice revealed no statistically significant overlap (Figure 5B). The 452 genes with significantly reduced H3K4me3 in both Kmt2a cKO and CK-p25 mice are almost exclusively enriched in memory- and synaptic-plasticity-related categories (Figures 5C and 5E). Interestingly, in the RNA-seq data of Gjoneska et al. (2015), *Kmt2a*, but not *Kmt2b*, is downregulated in CK-p25 mice (Figure 5F, upper panel). We confirmed this observation by qPCR (Figure 5F, lower panel).

Figure 2. Kmt2a and Kmt2b Distinctly Affect Hippocampal Histone-Methylation

(A) H3K4me3 levels are decreased in CA neurons of Kmt2a cKO mice (n = 3) compared to controls (n = 5). (Inset) Quantification of H3K4me3 enrichment around TSS regions is shown (±2,000 bp).

(B) H3K4me3 levels are decreased in CA neurons of Kmt2b cKO mice (n = 5) compared to controls (n = 7). (Inset) Quantification of H3K4me3 enrichment around TSS regions is shown (±2,000 bp).

(C) Number of unique genes differentially bound (FDR < 0.1 and fold change > 1.2) by H3K4me3 at their TSS regions (±2,000 bp) in Kmt2a cKO and Kmt2b cKO neurons (top). There is a substantial divergence between genes with decreased H3K4me3 in Kmt2a cKO and Kmt2b cKO mice (bottom).

(D and E) Genes with decreased H3K4me3 mostly fall under different functional categories (weighted p value < 0.001) in Kmt2a cKO (D) and Kmt2b cKO (E) mice.

(F) A representative set of TSS regions (±2,000 bp) with decreased H3K4me3 in Kmt2a cKO and Kmt2b cKO mice.

(G) TSS regions with decreased H3K4me3 in Kmt2a cKO and Kmt2b cKO mice possess unique consensus sequences.

(H) Representation of the number of TSS regions with significantly (FDR < 0.1) decreased H3K4me3 at different fold change thresholds in Kmt2a cKO and Kmt2b cKO mice. In this analysis, we quantified the total number of peaks within the TSS regions (±2,000 bp), whereas, in the data shown in (C), we consolidate the peaks into the number of genes.

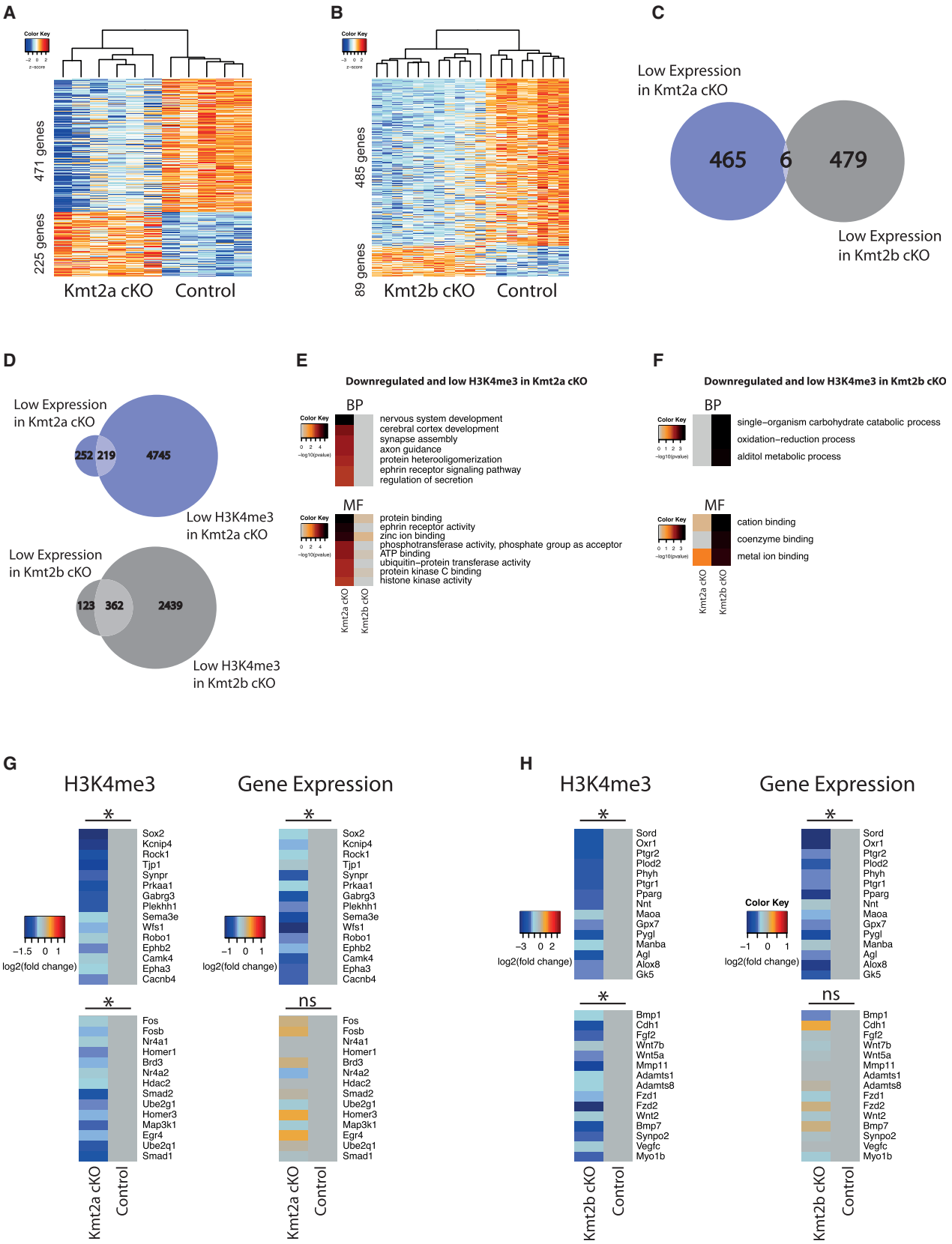

(legend on next page)

DISCUSSION

Kmt2b cKO mice have recently been shown to exhibit memory impairment (Kerimoglu et al., 2013). Here, we demonstrate that deletion of Kmt2a in the adult forebrain also impairs memory function. These findings concord with a study on constitutive heterozygous knockout of Kmt2a in mice, which exhibit impaired contextual fear memory (Gupta et al., 2010). However, the results regarding fear memory may at least partly be affected by decreased anxiety. Nevertheless, the fact that Kmt2a knockdown also impairs spatial memory in the water maze test argues for its essential involvement in hippocampus-dependent memory function. In support of this view, Kmt2a has previously been implicated in working memory (Jakovcevski et al., 2015), anxiety and addiction (Shen et al., 2016), and postnatal neurogenesis. Interestingly, although Kmt2b cKO mice display impaired object recognition memory (Kerimoglu et al., 2013), this specific form of memory is intact in Kmt2a cKO mice. These data are in line with findings for histone acetyltransferases (HATs). For example, CREB binding protein (CBP) is a HAT mainly linked to object recognition memory (Valor et al., 2011), whereas loss of other HATs, such as KAT2a/GCN5, does not affect this type of learning but rather causes impairment of spatial memory (Stilling et al., 2014). These data suggest that related histone-modifying enzymes are likely to control different transcriptional programs in postmitotic neurons. In line with this hypothesis, we observe that the closely related KMTs, Kmt2a and Kmt2b, appear to regulate different gene sets in hippocampal neurons, which is corroborated by the affected promoters having unique consensus sequences. These findings are based on H3K4me3 ChIP-seq experiments. Whereas we were unable to identify commercially available antibody to perform ChIP-seq for KMT2A and KMT2B in our experimental setting, data available from other cell types using, for example, tagged proteins suggest that both enzymes are found on a large number of overlapping promoters (Denissov et al., 2014; Guenther et al., 2005). These data indicate that the analysis of neuronal H3K4me3 ChIP-seq in mice that lack the H3K4me3 methlytransferases Kmt2a or Kmt2b in neurons of the adult brain is a reliable indicator of functionality of these enzymes. It is possible that the observed functional specificity of Kmt2a and Kmt2b is—at least in part—linked to specific protein interactions or posttranslational modifications and do not necessarily have to involve Kmt2a and Kmt2b binding to unique genomic locations. In line with this view, it was, for example, recently shown that protein kinase Msk1 can control Kmt2a-dependent gene expression (Wiersma et al., 2016). Moreover, there is evidence that the association with different co-activators can explain unique function of different subgroups of H3K4 methyltransferases—i.e., trx- (Kmt2a/b), trr- (Kmt2c/d), and Set1-related (Setd1a/b) (Duncan et al., 2015; Lee et al., 2006). For example, Kmt2c/d associate with ASC-2 (Lee et al., 2006), whereas Kmt2a/b bind to Menin (Dreijerink et al., 2006; Hughes et al., 2004; Shilatifard, 2012; Yokoyama et al., 2004). We suggest that future studies should address these issues.

Another interesting observation is that loss of neuronal Kmt2a and Kmt2b caused decreased H3K4me3 at a number of genomic regions without affecting corresponding gene expression. Although this observation is in line with previous studies carried out in adult and embryonic tissues (Denissov et al., 2014; Glaser et al., 2006; Jakovcevski et al., 2015; Kerimoglu et al., 2013; Shen et al., 2014), this may partly be due to ChIP-seq having been performed from neurons and RNA-seq from whole tissue.

Nevertheless, especially IEGs showed decreased H3K4me3 without concomitant downregulation, suggesting that Kmt2a and Kmt2b control activity-induced gene expression in neurons. This view is supported by findings in immune cells showing that only genes with high H3K4me3 at the TSS can be induced by histone deacetylase (HDAC) inhibitors (Wang et al., 2009), which are in turn known to improve memory (Fischer, 2014).

Our data also revealed that especially Kmt2a is required for neuronal H3K4me1. Genomic regions with decreased H3K4me1 in Kmt2a cKO mice were substantially different from those with decreased H3K4me3, which is in line with the view that H3K4me1 is an enhancer mark (Heintzman et al., 2009). Regions with reduced H3K4me1 are linked through long-distance interactions to chromosomal regions containing genes involved in transcriptional regulation, chromatin binding, and synaptic signaling/plasticity. These observations have to be interpreted with care, however, because the information regarding TADs is based on data from the mouse cortex (Dixon et al., 2012), because data from adult hippocampal neurons is not yet available. Nevertheless, the fact that chromosomal regions interacting with decreased H3K4me1 peaks are overrepresented for genes linked to synaptic signaling signifies the necessity to further explore the role of neuronal Kmt2a in long-distance interactions. These data indicate that Kmt2a elicits a dual impact on gene regulation in neuronal cells, through regulation of H3K4me3 and H3K4me1 at distinct genomic locations.

Figure 3. Kmt2a and Kmt2b Distinctly Affect Hippocampal Gene Expression

(A) Heatmap depicting significantly (FDR < 0.1 and fold change > 1.2) de-regulated genes in Kmt2a cKO mice (n = 5) compared to controls (n = 6).

(B) Heatmap depicting significantly (FDR < 0.1 and fold change > 1.2) de-regulated genes in Kmt2b cKO mice (n = 11) compared to controls (n = 8).

(C) Genes downregulated in both cKO mice are overwhelmingly unique.

(D) Venn diagrams depicting the overlap between TSS regions with decreased H3K4me3 and downregulated genes in Kmt2a cKO and Kmt2b cKO mice.

(E and F) Genes with concomitant downregulation and decrease in H3K4me3 in Kmt2a cKO (E) and Kmt2b cKO (F) mice fall under unique functional categories (weighted p value < 0.001).

(G) Depiction of H3K4me3 levels at TSS (left) and expression (right) of representative genes in Kmt2a cKO mice. Genes involved in neuronal development and synaptic signaling mostly manifest a concomitant decrease in H3K4me3 and expression (upper half), whereas those involved in chromatin remodeling and transcriptional regulation (many IEGs among them) have decreased H3K4me3 at their TSS without a concomitant change in expression (lower half).

(H) Depiction of H3K4me3 levels at TSS (left) and expression (right) of representative genes in Kmt2b cKO mice. Genes involved in oxidation reduction mostly manifest a concomitant decrease in H3K4me3 and expression (upper half), whereas those involved in cell adhesion and neuronal protrusion-related processes have decreased H3K4me3 at their TSS without a concomitant change in expression (lower half).

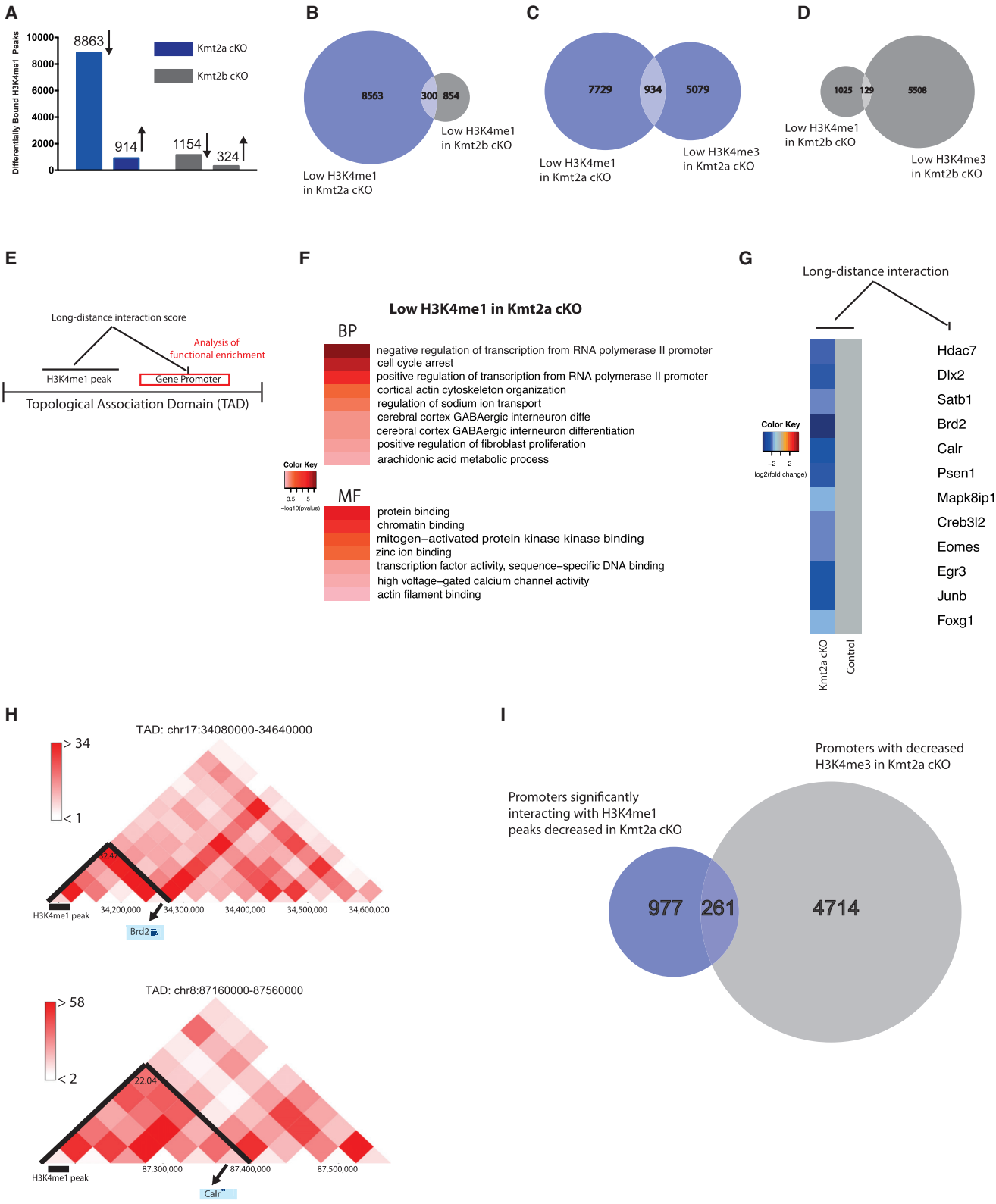

(legend on next page)

A possible mechanism through which Kmt2a can mediate H3K4me1 and H3K4me3 at different places may be its association with specific proteins at different genomic locations. Future studies should address this issue.

Interestingly, the genes affected by decreased H3K4me3 in hippocampal CA neurons of Kmt2a cKO mice showed a significant overlap to the changes observed in CK-p25 mice, a model for Alzheimer's disease (Fischer et al., 2005). This overlap and the number of promoters with decreased H3K4me3 in CK-p25 may even be underestimated, because Gjoneska et al. (2015) analyzed whole hippocampal tissue whereas we performed ChIP-seq experiments in hippocampal CA neurons. In contrast, the pattern in Kmt2b cKO mice was rather distinct from that in CK-p25 mice. In line with this, we observed that the *Kmt2a* gene is downregulated in the hippocampus of CK-p25 mice, whereas *Kmt2b* expression was not affected. Thus, our data suggest that dysfunction of Kmt2a-mediated H3K4 methylation might play a role in the pathogenesis of neurodegenerative diseases, such as Alzheimer's disease (AD), a hypothesis that should be further tested in future research.

EXPERIMENTAL PROCEDURES

For details, refer to Supplemental Experimental Procedures.

Animals

All mice used in this study were C57BL/6J mice of 3–5 months of age (C57B/6J). All groups were age and sex matched. Statistical analysis confirmed that no gender differences were observed in any experiment. Mice were kept in standard single cages with food and water provided ad libitum. In all experiments, mice containing loxP sites, but not expressing the Cre transgene, were used as controls. All experiments were performed in accordance with the animal protection law of the state of Lower Saxony (protocol number Fischer 1000/1004).

Behavioral Analysis

Both control and cKO groups contained male and female mice. The groups were age and sex matched. Statistical analysis revealed that there were no differences among groups due to gender.

In open-field and novel object recognition tests, mice were habituated to the plastic arena for 2 days for 5 min each. The relative time spent in the center was used as a readout of anxiety (i.e., open-field test). Afterward, the mice were habituated to two white boxes for 2 consecutive days and on the next day were presented with two black cubes. They were left to explore them for 5 min. After 24 hr, the one black cube was exchanged to a red tape. They explored the objects for 5 min, and the relative exploration time of the novel object (i.e., red tape) was used as an index of memory performance.

Elevated plus Maze Test

The mice were introduced for 5 min into the center of a plus maze with two open and two closed arms. The relative time spent in open arms was used as anxiety index.

Porsolt Forced Swim Test

Mice were introduced for 5 min into a container filled with water. Immobility time was measured.

Pavlovian Fear-Conditioning Test

Mice were introduced into a chamber and left to explore it for 3 min. Immediately afterward, they received a mild foot shock (0.5 mA) for 2 s. 24 hr later, they were reintroduced into the same chamber and their freezing behavior was measured.

Morris Water Maze Test

The setup consisted of a circular pool filled with opaque water into which a platform was submerged. At each training session, mice were introduced into the pool four times and were left to search for the hidden platform for 60 s. In cases where they were not able to find the platform within that time limit, they were gently guided there. Probe test was carried out 24 hr after the last training session.

Real-Time qPCR

RNA isolation was performed using TRIZOL (Invitrogen) as described previously (Kerimoglu et al., 2013). cDNA was synthesized with Transcriptor High Fidelity cDNA Synthesis Kit (Roche). All reactions were performed in Roche 480 Light Cycler.

Western Blotting

Protein isolation was performed using TriPrep kit from Macherey Nagel. Western blot for Kmt2a protein and bulk H3K4me3 in hippocampus was performed as described previously (Kuczera et al., 2010; Stilling et al., 2014).

Chromatin Immunoprecipitation from FACS-Sorted Nuclei

FACS

ChIP from neuronal and non-neuronal nuclei sorted by FACS was performed as described previously (Halder et al., 2016) with slight modifications.

ChIP

In order to obtain enough chromatin for ChIP experiments (500 ng at least), two samples of the same genotype and sex were combined throughout all experiments. 500 ng of chromatin was used for ChIP, and 50 ng of additional chromatin was used as input from each sample. The following antibodies were used for ChIP: H3K4me3: Abcam ab8580; H3K4me1: Abcam ab8895; and H3: Abcam ab1791. In all cases, 0.5 μg of antibody was used. ChIP was performed as described previously (Benito et al., 2015).

ChIP Sequencing

ChIP sequencing was performed as described previously (Benito et al., 2015; Halder et al., 2016).

RNA Sequencing

RNA sequencing was performed as described previously (Halder et al., 2016).

Figure 4. Kmt2a and Kmt2b-Dependent Histone 3 Lysine 4 Monomethylation

(A) Number of genomic regions differentially bound (FDR < 0.1 and fold change > 1.2) by H3K4me1 in Kmt2a cKO and Kmt2b cKO neurons.
(B) There is a substantial divergence between genomic regions with decreased (FDR < 0.1 and fold change > 1.2) H3K4me1 in Kmt2a cKO and Kmt2b cKO mice.
(C and D) There is also a substantial divergence between genomic regions with decreased H3K4me1 and H3K4me3 in both Kmt2a cKO (C) and Kmt2b cKO (D) mice.
(E) Depiction of the analysis of long-distance chromatin interactions mediated by peaks with decreased H3K4me1 using TAD information from Dixon et al. (2012). H3K4me1 peaks with significant interaction were subjected to GO enrichment analysis.
(F) Functional categories significantly (weighted p value < 0.001) affected by decreased H3K4me1 in Kmt2a cKO mice.
(G) Depiction of representative regions with decreased H3K4me1 in Kmt2a cKO mice and the gene promoters they presumably interact with.
(H) Representative depictions of long-distance chromatin interactions affected by reduced H3K4me1 in Kmt2a cKO neurons.
(I) Overlap between promoters with decreased H3K4me3 (FDR < 0.1 and fold change > 1.2) and those interacting with decreased H3K4me1 peaks (FDR < 0.1 and fold change > 1.2) in Kmt2a cKO neurons.

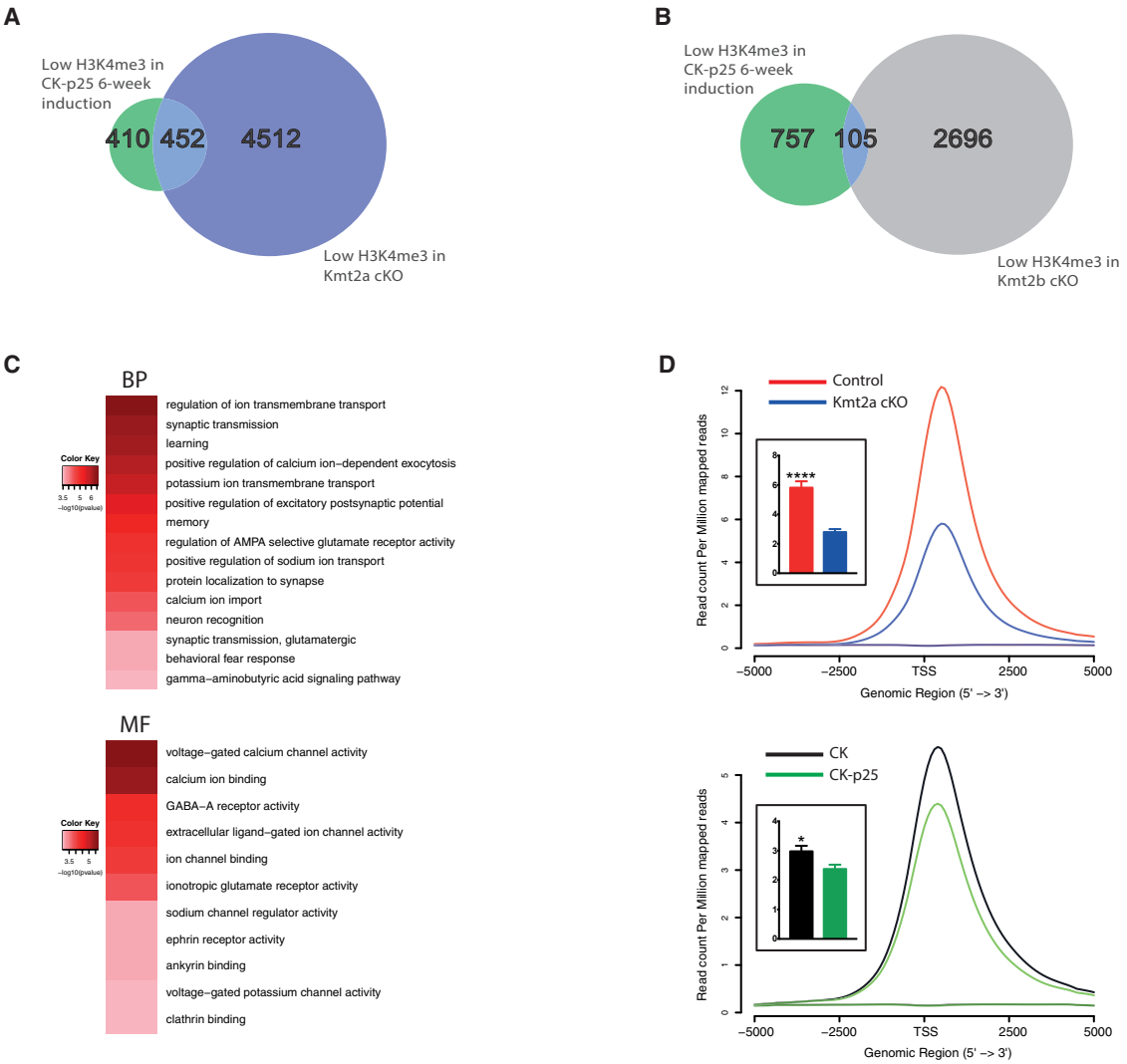

(legend on next page)

Statistical Analysis

Behavioral results were analyzed with two-way ANOVA in order to control for possible confounding effects of sex and/or interaction between sex and genotype. For analysis of ChIP and RNA sequencing results, see Supplemental Information. In all other comparisons, Student's t test was implemented unless indicated otherwise. Error bars in graphs represent SEM.

ACCESSION NUMBERS

The accession number for the ChIP-seq and RNA-seq data reported in this paper is GEO: GSE99250.

SUPPLEMENTAL INFORMATION

Supplemental Information includes Supplemental Experimental Procedures, six figures, and two data files and can be found with this article online at http://dx.doi.org/10.1016/j.celrep.2017.06.072.

AUTHOR CONTRIBUTIONS

C.K. and A.F. designed the research; A.K. and A.F.S. provided Kmt2a$^{f/f}$ and Kmt2b$^{f/f}$ mice; C.K., M.S.S., E.B., S.B., L.K., R.H., R.C.A.-B., R.S., and H.U. performed research; C.K. analyzed the data; G.J. performed the analysis with long-distance interactions involving TADs; V.C. performed qc analysis and alignment; and C.K. and A.F. wrote the paper. All authors read and approved the final manuscript.

ACKNOWLEDGMENTS

A.F. was supported by an ERC consolidator grant (DEPICODE; 648898), Deutsche Forschungsgemeinschaft (DFG) projects (FI981/6-1 and FI981/9-1), the JPND project RiMOD (grant 01ED1407), and funds to the German Center for Neurodegenerative Diseases (DZNE) from the Helmholtz Society. A.F.S. and A.K. were supported by the Deutsche Forschungsgemeinschaft (KR2154/3-1) and the Else Kröner-Fresenius-Stiftung (2012_A300). R.C.A.-B. was supported by the Ramón and Cajal (RYC-2014-15246) and the Galician Innovation Agency—GAIN (IN607D-2016/003) grants.

Received: December 15, 2016
Revised: April 9, 2017
Accepted: June 23, 2017
Published: July 18, 2017

REFERENCES

Andreu-Vieyra, C.V., Chen, R., Agno, J.E., Glaser, S., Anastassiadis, K., Stewart, A.F., and Matzuk, M.M. (2010). MLL2 is required in oocytes for bulk histone 3 lysine 4 trimethylation and transcriptional silencing. PLoS Biol. *8*, e1000453.

Benito, E., Urbanke, E., Ramachandran, B., Barth, J., Halder, R., Awasthi, A., Jain, G., Capece, V., Burkhardt, S., Navarro-Sala, M., et al. (2015). HDAC inhibitor-dependent transcriptome and memory reinstatement in cognitive decline models. J. Clin. Invest. *125*, 3572–3584.

Day, J.J., and Sweatt, J.D. (2011). Epigenetic mechanisms in cognition. Neuron *70*, 813–829.

Denissov, S., Hofemeister, H., Marks, H., Kranz, A., Ciotta, G., Singh, S., Anastassiadis, K., Stunnenberg, H.G., and Stewart, A.F. (2014). Mll2 is required for H3K4 trimethylation on bivalent promoters in embryonic stem cells, whereas Mll1 is redundant. Development *141*, 526–537.

Dixon, J.R., Selvaraj, S., Yue, F., Kim, A., Li, Y., Shen, Y., Hu, M., Liu, J.S., and Ren, B. (2012). Topological domains in mammalian genomes identified by analysis of chromatin interactions. Nature *485*, 376–380.

Dreijerink, K.M., Mulder, K.W., Winkler, G.S., Höppener, J.W., Lips, C.J., and Timmers, H.T. (2006). Menin links estrogen receptor activation to histone H3K4 trimethylation. Cancer Res. *66*, 4929–4935.

Duncan, E.M., Chitsazan, A.D., Seidel, C.W., and Sánchez Alvarado, A. (2015). Set1 and MLL1/2 target distinct sets of functionally different genomic loci in vivo. Cell Rep. *13*, 2741–2755.

Fischer, A. (2014). Epigenetic memory: the Lamarckian brain. EMBO J. *33*, 945–967.

Fischer, A., Sananbenesi, F., Pang, P.T., Lu, B., and Tsai, L.H. (2005). Opposing roles of transient and prolonged expression of p25 in synaptic plasticity and hippocampus-dependent memory. Neuron *48*, 825–838.

Gjoneska, E., Pfenning, A.R., Mathys, H., Quon, G., Kundaje, A., Tsai, L.H., and Kellis, M. (2015). Conserved epigenomic signals in mice and humans reveal immune basis of Alzheimer's disease. Nature *518*, 365–369.

Glaser, S., Schaft, J., Lubitz, S., Vintersten, K., van der Hoeven, F., Tufteland, K.R., Aasland, R., Anastassiadis, K., Ang, S.L., and Stewart, A.F. (2006). Multiple epigenetic maintenance factors implicated by the loss of Mll2 in mouse development. Development *133*, 1423–1432.

Guenther, M.G., Jenner, R.G., Chevalier, B., Nakamura, T., Croce, C.M., Canaani, E., and Young, R.A. (2005). Global and Hox-specific roles for the MLL1 methyltransferase. Proc. Natl. Acad. Sci. USA *102*, 8603–8608.

Gupta, S., Kim, S.Y., Artis, S., Molfese, D.L., Schumacher, A., Sweatt, J.D., Paylor, R.E., and Lubin, F.D. (2010). Histone methylation regulates memory formation. J. Neurosci. *30*, 3589–3599.

Halder, R., Hennion, M., Vidal, R.O., Shomroni, O., Rahman, R.U., Rajput, A., Centeno, T.P., van Bebber, F., Capece, V., Garcia Vizcaino, J.C., et al. (2016). DNA methylation changes in plasticity genes accompany the formation and maintenance of memory. Nat. Neurosci. *19*, 102–110.

Heintzman, N.D., Hon, G.C., Hawkins, R.D., Kheradpour, P., Stark, A., Harp, L.F., Ye, Z., Lee, L.K., Stuart, R.K., Ching, C.W., et al. (2009). Histone modifications at human enhancers reflect global cell-type-specific gene expression. Nature *459*, 108–112.

Hughes, C.M., Rozenblatt-Rosen, O., Milne, T.A., Copeland, T.D., Levine, S.S., Lee, J.C., Hayes, D.N., Shanmugam, K.S., Bhattacharjee, A., Biondi, C.A., et al. (2004). Menin associates with a trithorax family histone methyltransferase complex and with the hoxc8 locus. Mol. Cell *13*, 587–597.

Figure 5. Histone-Methylation Changes in Kmt2a, Kmt2b, and CK-p25 Mice

(A) The overlap between genes with decreased (FDR < 0.1 and fold change < −1.2) H3K4me3 at TSS in Kmt2a cKO and 6-week induced CK-p25 mice (hypergeometric test: p value < 0.0001).

(B) The overlap between genes with decreased (FDR < 0.1 and fold change < −1.2) H3K4me3 at TSS in Kmt2b cKO and 6-week induced CK-p25 mice (hypergeometric test: p value = 1).

(C) Genes with decreased H3K4me3 in both Kmt2a cKO and CK-p25 mice are enriched in biological process (BP) and molecular function (MF) categories related to learning and memory and synaptic plasticity.

(D) H3K4me3 profile plots of overlapping genes from (A) in Kmt2a cKO (upper panel) and CK-p25 (lower panel) mice. (Inset) Quantification of H3K4me3 enrichment at TSS regions is shown (±2,000 bp). Error bars indicate SEM.

(E) Genome browser views of H3K4me3 enrichment along representative overlapping genes from (A) in Kmt2a cKO mice (upper two rows: H3K4me3 ChIP; lower two rows: input).

(F) Changes in *Kmt2a* and *Kmt2b* expression in CK-p25 mice; (upper panel) RNA-seq results from Gjoneska et al. (2015); (lower panel) qPCR results in our batch of CK-p25 mice (*p < 0.05).

Jakovcevski, M., and Akbarian, S. (2012). Epigenetic mechanisms in neurological disease. Nat. Med. *18*, 1194–1204.

Jakovcevski, M., Ruan, H., Shen, E.Y., Dincer, A., Javidfar, B., Ma, Q., Peter, C.J., Cheung, I., Mitchell, A.C., Jiang, Y., et al. (2015). Neuronal Kmt2a/Mll1 histone methyltransferase is essential for prefrontal synaptic plasticity and working memory. J. Neurosci. *35*, 5097–5108.

Kerimoglu, C., Agis-Balboa, R.C., Kranz, A., Stilling, R., Bahari-Javan, S., Benito-Garagorri, E., Halder, R., Burkhardt, S., Stewart, A.F., and Fischer, A. (2013). Histone-methyltransferase MLL2 (KMT2B) is required for memory formation in mice. J. Neurosci. *33*, 3452–3464.

Kuczera, T., Stilling, R.M., Hsia, H.E., Bahari-Javan, S., Irniger, S., Nasmyth, K., Sananbenesi, F., and Fischer, A. (2010). The anaphase promoting complex is required for memory function in mice. Learn. Mem. *18*, 49–57.

Lee, S., Lee, D.K., Dou, Y., Lee, J., Lee, B., Kwak, E., Kong, Y.Y., Lee, S.K., Roeder, R.G., and Lee, J.W. (2006). Coactivator as a target gene specificity determinant for histone H3 lysine 4 methyltransferases. Proc. Natl. Acad. Sci. USA *103*, 15392–15397.

Minichiello, L., Korte, M., Wolfer, D., Kühn, R., Unsicker, K., Cestari, V., Rossi-Arnaud, C., Lipp, H.P., Bonhoeffer, T., and Klein, R. (1999). Essential role for TrkB receptors in hippocampus-mediated learning. Neuron *24*, 401–414.

Mohan, M., Herz, H.M., Smith, E.R., Zhang, Y., Jackson, J., Washburn, M.P., Florens, L., Eissenberg, J.C., and Shilatifard, A. (2011). The COMPASS family of H3K4 methylases in Drosophila. Mol. Cell. Biol. *31*, 4310–4318.

Roguev, A., Schaft, D., Shevchenko, A., Pijnappel, W.W., Wilm, M., Aasland, R., and Stewart, A.F. (2001). The Saccharomyces cerevisiae Set1 complex includes an Ash2 homologue and methylates histone 3 lysine 4. EMBO J. *20*, 7137–7148.

Shen, E., Shulha, H., Weng, Z., and Akbarian, S. (2014). Regulation of histone H3K4 methylation in brain development and disease. Philos. Trans. R. Soc. Lond. B Biol. Sci. *369*, 20130514.

Shen, E.Y., Jiang, Y., Javidfar, B., Kassim, B., Loh, Y.E., Ma, Q., Mitchell, A.C., Pothula, V., Stewart, A.F., Ernst, P., et al. (2016). Neuronal deletion of Kmt2a/Mll1 histone methyltransferase in ventral striatum is associated with defective spike-timing-dependent striatal synaptic plasticity, altered response to dopaminergic drugs, and increased anxiety. Neuropsychopharmacology *41*, 3103–3113.

Shilatifard, A. (2012). The COMPASS family of histone H3K4 methylases: mechanisms of regulation in development and disease pathogenesis. Annu. Rev. Biochem. *81*, 65–95.

Stilling, R.M., Rönicke, R., Benito, E., Urbanke, H., Capece, V., Burkhardt, S., Bahari-Javan, S., Barth, J., Sananbenesi, F., Schütz, A.L., et al. (2014). K-lysine acetyltransferase 2a regulates a hippocampal gene expression network linked to memory formation. EMBO J. *33*, 1912–1927.

Valor, L.M., Pulopulos, M.M., Jimenez-Minchan, M., Olivares, R., Lutz, B., and Barco, A. (2011). Ablation of CBP in forebrain principal neurons causes modest memory and transcriptional defects and a dramatic reduction of histone acetylation but does not affect cell viability. J. Neurosci. *31*, 1652–1663.

Wang, Z., Zang, C., Cui, K., Schones, D.E., Barski, A., Peng, W., and Zhao, K. (2009). Genome-wide mapping of HATs and HDACs reveals distinct functions in active and inactive genes. Cell *138*, 1019–1031.

Wiersma, M., Bussiere, M., Halsall, J.A., Turan, N., Slany, R., Turner, B.M., and Nightingale, K.P. (2016). Protein kinase Msk1 physically and functionally interacts with the KMT2A/MLL1 methyltransferase complex and contributes to the regulation of multiple target genes. Epigenetics Chromatin *9*, 52.

Yokoyama, A., Wang, Z., Wysocka, J., Sanyal, M., Aufiero, D.J., Kitabayashi, I., Herr, W., and Cleary, M.L. (2004). Leukemia proto-oncoprotein MLL forms a SET1-like histone methyltransferase complex with menin to regulate Hox gene expression. Mol. Cell. Biol. *24*, 5639–5649.

Cell Reports, Volume *20*

Supplemental Information

KMT2A and KMT2B Mediate Memory Function by Affecting Distinct Genomic Regions

Cemil Kerimoglu, M. Sadman Sakib, Gaurav Jain, Eva Benito, Susanne Burkhardt, Vincenzo Capece, Lalit Kaurani, Rashi Halder, Roberto Carlos Agís-Balboa, Roman Stilling, Hendrik Urbanke, Andrea Kranz, A. Francis Stewart, and Andre Fischer

SUPPLEMENTAL INFORMATION

Experimental Procedures

Animals

The generation of mutant mice harboring floxed alleles for Kmt2a cKO and Kmt2b cKO mice was described previously (Denissov et al., 2014; Glaser et al., 2006; Minichiello et al., 1999) and crossing of these mutant mice with CamKII-Cre mice (Minichiello et al., 1999) has also been described in our previous studies (Kerimoglu et al., 2013).

Quantitative Real-Time PCR

Knockdown of *Kmt2a* at the mRNA level and decrease in H3K4me3 at Synpr and Robo1 promoters was confirmed by quantitative real-time PCR (qRT-PCR) and chromatin immunoprecipitation (ChIP) followed by qRT-PCR respectively, using SYBR Green. Decrease in expression of some candidate genes in Kmt2a cKO mice was confirmed by qRT-PCR using probes from Roche Universal Probe Library (UPL). In the case of qRT-PCR from cDNA results were normalized to hypoxanthine phosphoribosyltransferase (*Hprt1*) gene (except in CK-p25 mice), whereas in qRT-PCR after ChIP normalization was done against input DNA. For qRT-PCR in CK-p25 mice ribosomal protein L13A (*Rpl13a*) was used as housekeeping gene.

The following primers were used:

Kmt2a forward: GCTCAGATGAAGAAGTCAGAG

Kmt2a reverse: GTAGAAACCTACTTCCCATGCC

Hprt1 forward: GACAGGGACTCACTGCATAGTTT

Hprt1 reverse: GAGGCCAAGACAAGAAGACG

Robo1 forward: AGGGAAGCCTACGCACATG

Robo1 reverse: TGGACAGTGGGCGATTTTAT

Hcn1 forward: CGCCTTTCAAGGTTAATCAGA

Hcn1 reverse: GGCGAGGTCATAGGTCATGT

Camk4 forward: CGATTTCTTCGAGGTGGAGT

Camk4 reverse: CCCCTTCTGTTTGCATCTGT

Wfs1 forward: GGTTTCGGAGCAACTTCG

Wfs1 reverse: GGTGCCTGAGTTCATCTTGC

Synpr forward: CACCTTTCGGGCATTGAA

Synpr reverse: TGTTGCAAATGCAAACATTG

Kcnb2 forward: CCGGAGAAACGGAAGAAAC

Kcnb2 reverse: ATAGACACGATGGCCAGGAT

Kmt2a forward: ATTGAATACGCCGGCAAC

Kmt2a reverse: GGAACATGTAGCAACCAATGC

Kmt2b forward: GGAGGAAGAGAGCAGTGACG

Kmt2b reverse: TCATCTGAATGAAAACCCTGAA

Rpl13a forward: ATCCCTCCACCCTATGACAA

Rpl13a reverse: GCCCCAGGTAAGCAAACTT

Synpr_promoter forward: TGCTGCTCTCCAGACTACATTCC

Synpr_promoter reverse: GCGTGGAAAGGCTTCTTGTAACT

Robo1_promoter forward: GTGGTGATAGTGGTAGTGAGTGA

Robo1_promoter reverse: CTCAGGTGAGATTTCAACGACTC

Nkapl_promoter forward: GCTCAAGGTGGGGAATGTAA

Nkapl_promoter reverse: CGCAGGCGCACTAGAGAC

Ap1s3_promoter forward: GCGCAGGTGTAAGCACTG

Ap1s3_promoter reverse: TCCTGGCTTCCTCAAATTGT

Prkra_promoter forward: TGACTACTGCAGGCGAAAGA

Prkra_promoter reverse: GGCATTGTCCTACGTCACAA

Western Blotting

The following antibodies were used: Kmt2a (Cell Signaling), H3K4me3 (Abcam), β-actin (Santa Cruz) and tubulin (Sigma). The membranes were treated with fluorescently labeled secondary antibodies (IRDye 800 anti-rabbit or anti-mouse). Immunoblots were visualized and quantified in Odyssey Imager (Licor).

Chromatin Immunoprecipitation from FACS-sorted Nuclei

FACS

Brain tissue was homogenized in 0.32 M sucrose buffer (0.32M sucrose, 5mM $CaCl_2$, 5mM $Mg(CH_3COO)_2$, 0.1mM EDTA, 10mM HEPES, pH 8.0, 1mM DTT, 0.1% Triton X-100) with protease inhibitors (Roche Complete) and crosslinked with 1% formaldehyde (Sigma-Aldrich) for 5 minutes. Crosslinking was stopped with 125 mM glycine and incubating for 5 more minutes. Cells were pelleted by centrifugation at 2000 rcf for 5 minutes and were re-suspended and homogenized again in 0.32 M sucrose buffer. The solution was carefully added on top of 1 M sucrose buffer (1M sucrose, 3mM $Mg(CH_3COO)_2$, 10mM HEPES pH 8.0, 1mM DTT) and centrifuged at 3100 rcf for 10 minutes at 4^oC. The nuclear pellet was dissolved in PBS and later incubated with NeuN antibody conjugated with AF488 (Millipore MAB 377X) for 20 minutes at 4^oC. The nuclei were pelleted by centrifugation at 2000 rcf for 5 minutes and washed twice with PBS-Tween (0.2%Tween-20 dissolved in PBS; pH 7.5) and stored in PBS-Tween with 5% BSA for sorting. They were filtered (70 μm) into ice-cold conical tubes containing 500 μl of PBS-Tween with 5% BSA right before sorting. Sorting was done on FACSAria II (BD Bioscience). NeuN stained (NeuN +) fractions were collected and were centrifuged at 3100 rcf for 10 minutes at 4^oC after sorting. The nuclear pellet was re-suspended in leftover supernatant, transferred to 1.5 mL microcentrifuge tubes (Eppendorf) and centrifuged at 10000 rcf for 5 min at 4^oC. Supernatant was discarded and the nuclei were flash frozen in liquid nitrogen and kept at -80^oC until further processing.

Chromatin Immunoprecipitation (ChIP)

Each sample was at first re-suspended in 75 μl of RIPA buffer (140 mM NaCl, 1 mM EDTA, 1% Triton X-100, 0.1% $C_{24}H_{39}NaO_4$, 10 mM Tris pH 8, 1% SDS) and then two were combined making 150 μl total. 150 μl samples were transferred to sonication tubes (Diagenode) and sonicated for 35 cycles (30 sec ON / 30 sec OFF) at setting “High” on Bioruptor Plus (Diagenode). To ensure homogenous shearing, samples were spun down every five cycles. Chromatin quantity and quality were measured with Qubit High Sensitivity dsDNA Assay Kit and Agilent 2100 Bioanalyzer High Sensitivity DNA Kit respectively. All samples contained more than 1000 ng of chromatin with the average size of at most 300 bp.

ChIP-Sequencing

Libraries were prepared using NEBNext Ultra DNA Library Prep Kit for Illumina (NEB) and were measured in QuBit and Agilent 2100 Bioanalyzer. Input DNA was isolated from every sample and was pooled for each group separately.

Base calling, conversion to fastq, quality control, read mapping to mouse genome (*Mus musculus* mm10) were done as described in (Halder et al., 2016) and (Narayanan et al., 2015). Filtering was done leaving only high quality reads (MAPQ ! = (0, 2, 3, 4)) as described in (Halder et al., 2016).

RNA-Sequencing

RNA quantity and quality were checked using Nanodrop and Agilent 2100 Bioanalyzer RNA kit respectively. All the RNA samples had a R.I.N. value above 8.0.

cDNA libraries were prepared with the TruSeq RNA Sample Preparation v2 Kit (Illumina). Library quantity was checked with Qubit dsDNA HS Assay kit and quality with Agilent 2100 Bioanalyzer.

Base calling, conversion to fastq, quality control, read mapping to mouse genome were performed in the same way as for ChIP-Seq. Reads were aligned to mouse genome *Mus musculus* mm10 and counted using FeaturesCount (http://bioinf.wehi.edu.au/featureCounts/) as described previously (Halder et al., 2016).

Data Analysis

Peak calling and differential binding analysis

Peak enrichment was performed with MACS2 using q-value < 0.1 (Feng et al., 2011) and differential binding was assessed using DiffBind package of Bioconductor (Ross-Innes et al., 2012) with in-built DESEQ2 option for differential analysis. Since mice of both sexes were used in experiments, sex was assigned as a blocking factor. Peak annotation was performed with HOMER (Heinz et al., 2010).

Differential expression analysis

Differential expression was analyzed using DESeq2 package of Bioconductor (Love et al., 2014). Again the effect of sex was controlled for during the analysis.

Genome-wide enrichment plots and visualization

merge function of samtools (Li et al., 2009) was used to combine BAM files of replicates of the same group into a single BAM file. These merged BAM files together with their respective input files were used to create profile plots of H3K4me3 with NGSPlot using non-default parameters (Shen et al., 2014).

H3K4me3 around TSS regions was visualized through the Integrated Genome Browser (Nicol et al., 2009) using wiggle files created from the merged BAM files with the script from the MEDIPS package of Bioconductor (Lienhard et al., 2014).

Functional enrichment analysis

Enrichment of functional GO categories was performed using topGO package of Bioconductor, using the weighted analysis option. GO categories with a weighted p-value below 0.001 were considered significant.

Analysis of overlaps between genomic regions

The extent of overlap between genomic regions was assessed using GenomicRanges package of Bioconductor (Lawrence et al., 2013). The options maxgap=0 and minoverlap=1 were used.

Motif discovery

Discovery of consensus sequences and target transcription factors was performed with MEME-ChIP (Bailey et al., 2009; Machanick and Bailey, 2011) using default parameters. Targets with E-value above 0.05 were considered significant.

Analysis of long-distance interactions

We obtained the Hi-C data and TAD boundary coordinates from Dixon, et al. (Dixon et al., 2012) (GEO: GSE35156). We calculated the interaction score between the ChIP peaks and TSS from the Hi-C interaction frequency within the same TADs. The interaction scores were then ranked from highest to lowest.

Supplemental References

Bailey, T.L., Boden, M., Buske, F.A., Frith, M., Grant, C.E., Clementi, L., Ren, J., Li, W.W., and Noble, W.S. (2009). MEME SUITE: tools for motif discovery and searching. Nucleic Acids Res *37*, W202-208.

Denissov, S., Hofemeister, H., Marks, H., Kranz, A., Ciotta, G., Singh, S., Anastassiadis, K., Stunnenberg, H.G., and Stewart, A.F. (2014). Mll2 is required for H3K4 trimethylation on bivalent promoters in embryonic stem cells, whereas Mll1 is redundant. Development *141*, 526-537.

Dixon, J.R., Selvaraj, S., Yue, F., Kim, A., Li, Y., Shen, Y., Hu, M., Liu, J.S., and Ren, B. (2012). Topological domains in mammalian genomes identified by analysis of chromatin interactions. Nature *485*, 376-380.

Feng, J., Liu, T., and Zhang, Y. (2011). Using MACS to identify peaks from ChIP-Seq data. Current protocols in bioinformatics *Chapter 2*, Unit 2 14.

Glaser, S., Schaft, J., Lubitz, S., Vintersten, K., van der Hoeven, F., Tufteland, K.R., Aasland, R., Anastassiadis, K., Ang, S.L., and Stewart, A.F. (2006). Multiple epigenetic maintenance factors implicated by the loss of Mll2 in mouse development. Development *133*, 1423-1432.

Halder, R., Hennion, M., Vidal, R.O., Shomroni, O., Rahman, R.U., Rajput, A., Centeno, T.P., van Bebber, F., Capece, V., Garcia Vizcaino, J.C*., et al.* (2016). DNA methylation changes in plasticity genes accompany the formation and maintenance of memory. Nature neuroscience *19*, 102-110.

Heinz, S., Benner, C., Spann, N., Bertolino, E., Lin, Y.C., Laslo, P., Cheng, J.X., Murre, C., Singh, H., and Glass, C.K. (2010). Simple combinations of lineage-determining transcription factors prime cis-regulatory elements required for macrophage and B cell identities. Mol Cell *38*, 576-589.

Kerimoglu, C., Agis-Balboa, R.C., Kranz, A., Stilling, R., Bahari-Javan, S., Benito-Garagorri, E., Halder, R., Burkhardt, S., Stewart, A.F., and Fischer, A. (2013). Histone-methyltransferase MLL2 (KMT2B) is required for memory formation in mice. The Journal of neuroscience : the official journal of the Society for Neuroscience *33*, 3452-3464.

Lawrence, M., Huber, W., Pages, H., Aboyoun, P., Carlson, M., Gentleman, R., Morgan, M.T., and Carey, V.J. (2013). Software for computing and annotating genomic ranges. PLoS computational biology *9*, e1003118.

Li, H., Handsaker, B., Wysoker, A., Fennell, T., Ruan, J., Homer, N., Marth, G., Abecasis, G., Durbin, R., and Genome Project Data Processing, S. (2009). The Sequence Alignment/Map format and SAMtools. Bioinformatics *25*, 2078-2079.

Lienhard, M., Grimm, C., Morkel, M., Herwig, R., and Chavez, L. (2014). MEDIPS: genome-wide differential coverage analysis of sequencing data derived from DNA enrichment experiments. Bioinformatics *30*, 284-286.

Love, M.I., Huber, W., and Anders, S. (2014). Moderated estimation of fold change and dispersion for RNA-seq data with DESeq2. Genome Biol *15*, 550.

Machanick, P., and Bailey, T.L. (2011). MEME-ChIP: motif analysis of large DNA datasets. Bioinformatics *27*, 1696-1697.

Minichiello, L., Korte, M., Wolfer, D., Kuhn, R., Unsicker, K., Cestari, V., Rossi-Arnaud, C., Lipp, H.P., Bonhoeffer, T., and Klein, R. (1999). Essential role for TrkB receptors in hippocampus-mediated learning. Neuron *24*, 401-414.

Narayanan, R., Pirouz, M., Kerimoglu, C., Pham, L., Wagener, R.J., Kiszka, K.A., Rosenbusch, J., Seong, R.H., Kessel, M., Fischer, A*., et al.* (2015). Loss of BAF (mSWI/SNF) Complexes Causes Global Transcriptional and Chromatin State Changes in Forebrain Development. Cell reports *13*, 1842-1854.

Nicol, J.W., Helt, G.A., Blanchard, S.G., Jr., Raja, A., and Loraine, A.E. (2009). The Integrated Genome Browser: free software for distribution and exploration of genome-scale datasets. Bioinformatics *25*, 2730-2731.

Ross-Innes, C.S., Stark, R., Teschendorff, A.E., Holmes, K.A., Ali, H.R., Dunning, M.J., Brown, G.D., Gojis, O., Ellis, I.O., Green, A.R*., et al.* (2012). Differential oestrogen receptor binding is associated with clinical outcome in breast cancer. Nature *481*, 389-393.

Shen, L., Shao, N., Liu, X., and Nestler, E. (2014). ngs.plot: Quick mining and visualization of next-generation sequencing data by integrating genomic databases. BMC genomics *15*, 284.

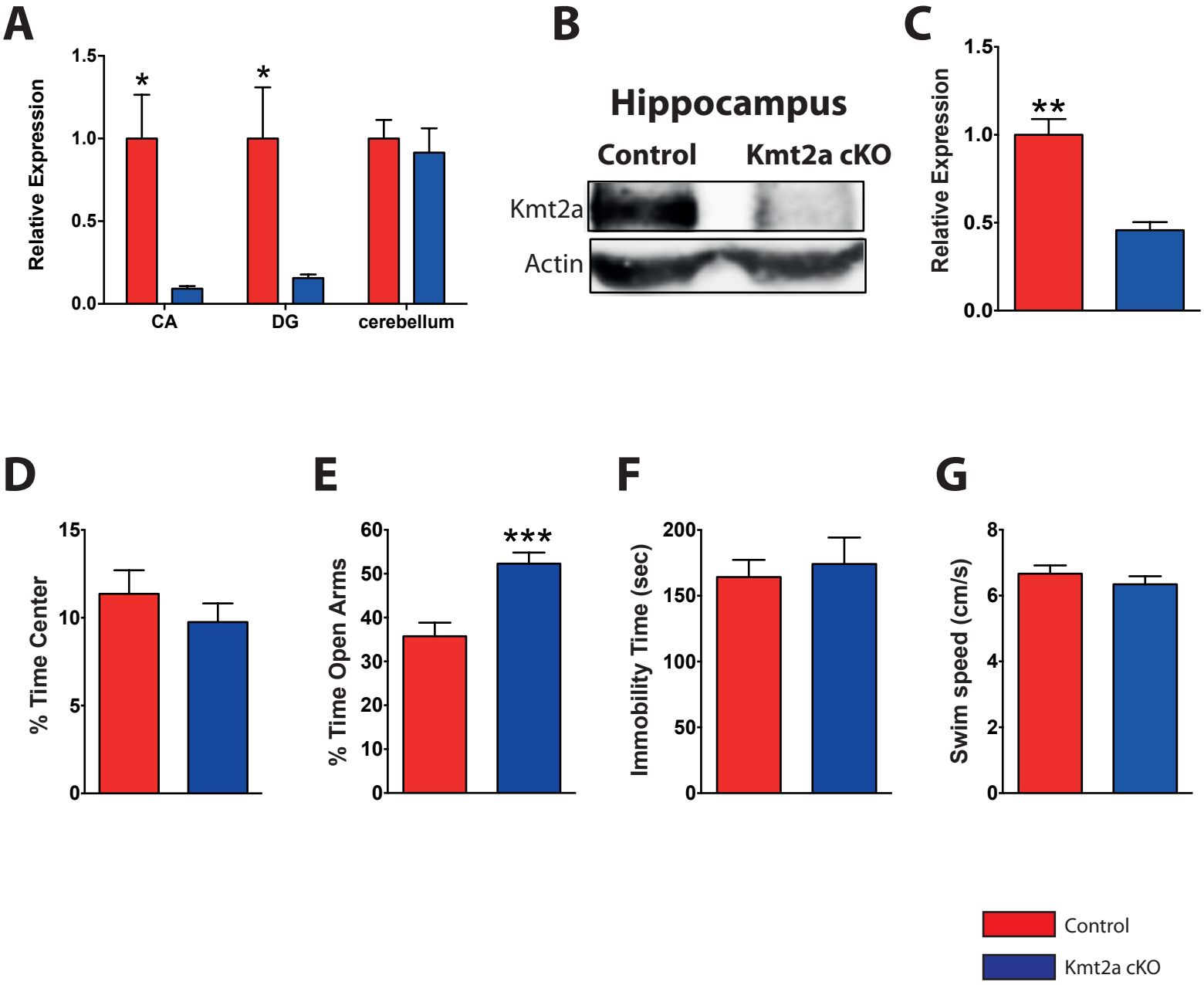

Figure S1, related to Figure 1: (A) mRNA of Kmt2a is decreased in hippocampal dentate gyrus (DG) (n=4/group) and CA (n=4/group) but not in cerebellum (control: n=4, Kmt2a cKO: n=3), as confirmed by qPCR (* $p < 0.05$). (B-C) Loss of Kmt2a protein in hippocampus was confirmed by western blot (control: n=4, Kmt2a cKO: n=3) (** $p < 0.01$). A representative image showing the Kmt2a and corresponding Actin band is shown. (D) Kmt2a cKO mice do not show any difference to controls in proportion of time spent in center of an open field (control n = 20, Kmt2a cKO n = 16). (E) Kmt2a cKO mice spend significantly more time in the open arms of elevated plus maze (*** $p < 0.001$; control n = 14, Kmt2a cKO n = 14). (F) Ktm2a cKO mice show no difference to controls in immobility time when subjected to forced swim test. (G) Kmt2a cKO and control mice had a similar swimming speed in water maze test (control n = 14, Kmt2a cKO n = 13).

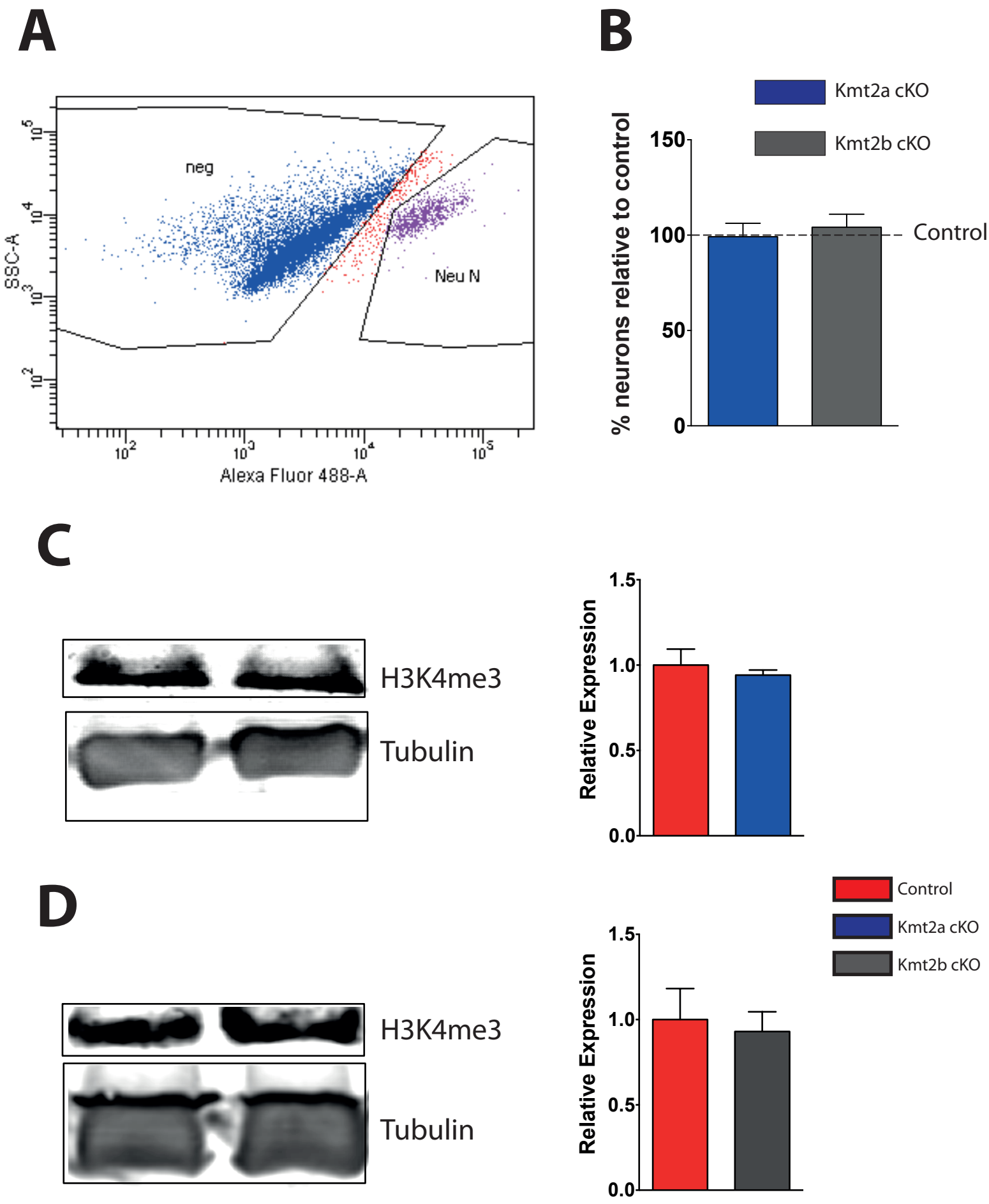

Figure S2, related to Figure 2: (A) Neurons, identified by NeuN staining, are clearly separated from non-neuronal cells by FACS. (B) Numbers of neurons in CA of both Kmt2a cKO and Kmt2b cKO mice are comparable to those in their respective control littermates. (C) There is no change in bulk H3K4me3 levels in CA of Kmt2a cKO mice (control: n=4, Kmt2a cKO: n=3). (D) There is no change in bulk H3K4me3 levels in CA of Kmt2b cKO mice (control: n=4, Kmt2b cKO: n=3). For C & D representative images are shown. Error bars indicate SEM.

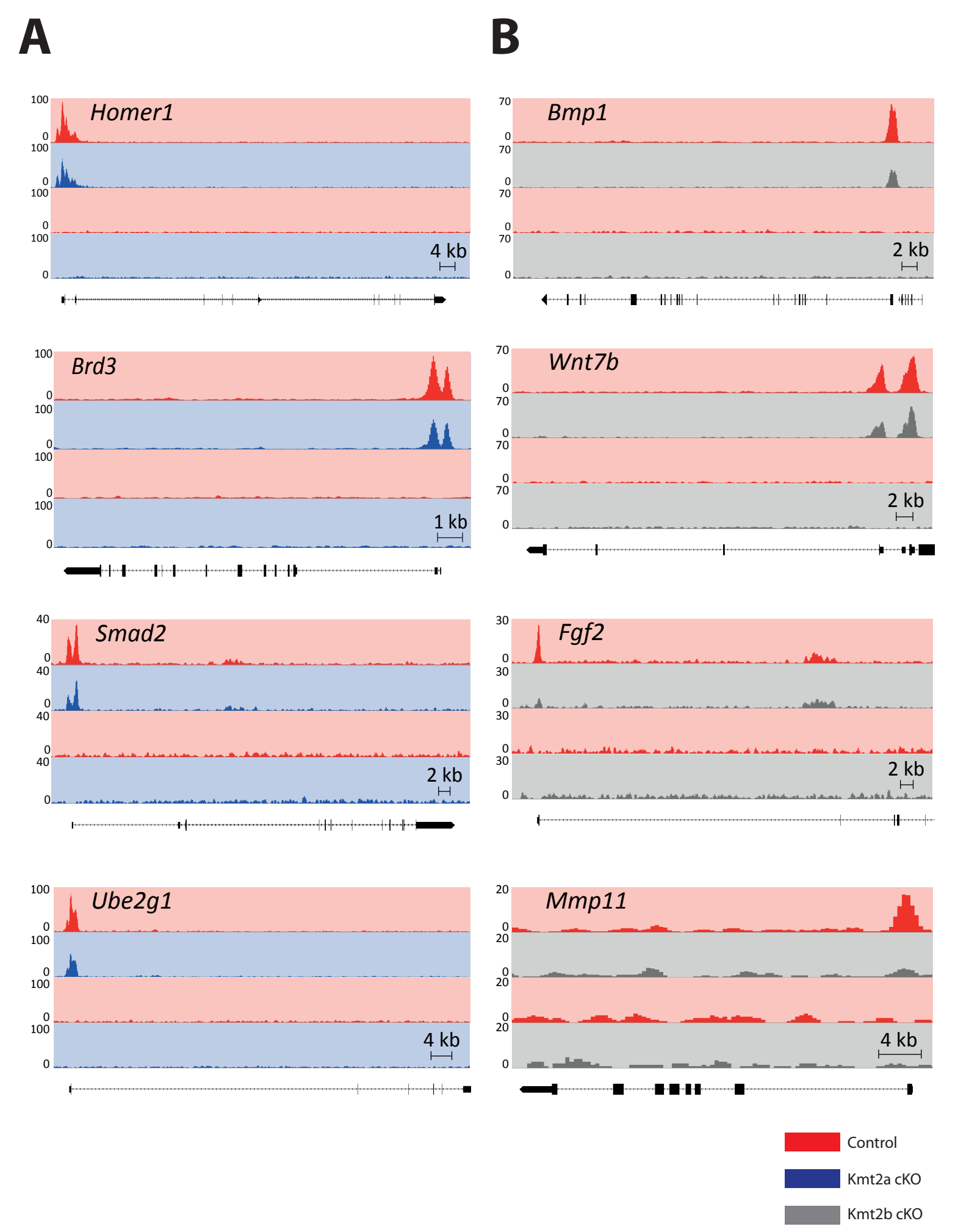

Figure S3, related to Figure 2: (A) Genome browser views of representativegenes with decreased H3K4me3 around TSS of Kmt2a cKO mice (upper two rows: H3K4me3 ChIP, lower two rows: input). (B) Genome browser views of representative genes with decreased H3K4me3 around TSS of Kmt2b cKO mice (upper two rows: H3K4me3 ChIP, lower two rows: input).

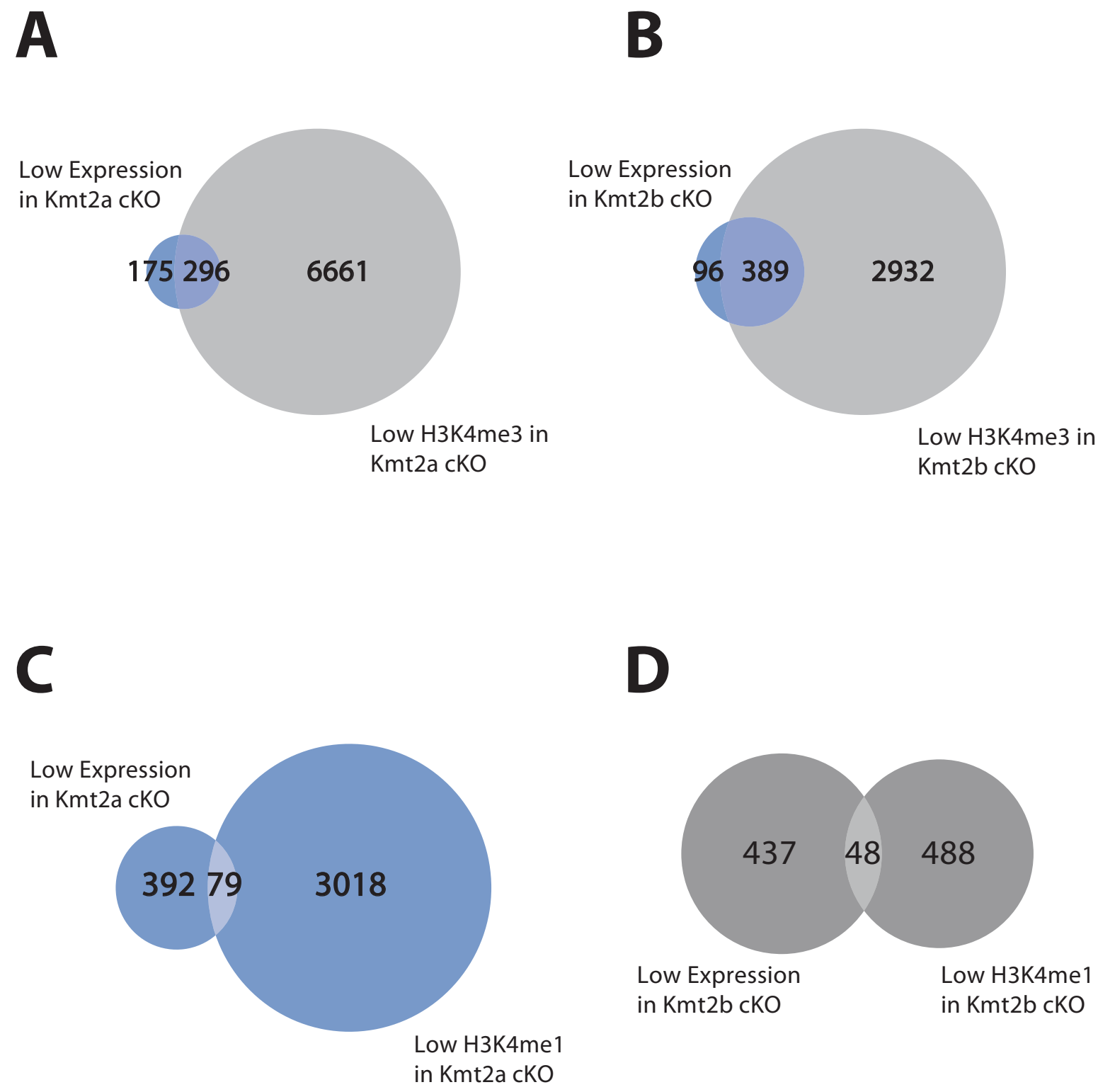

Figure S4: (A-B, related to Figure 3) Overlap between downregulated genes (FDR < 0.1 & fold change > 1.2) and decreased H3K4me3 at TSS regions with a more lenient treshold (FDR < 0.2 & fold change > 1.2) in Kmt2a cKO (A) and Kmt2b cKO (B) mice. (C-D, related to Figure 4) Venn diagrams depicting the overlap between TSS regions with decreased H3K4me1 and downregulated genes in Kmt2a cKO (C) and Kmt2b cKO (D) mice.

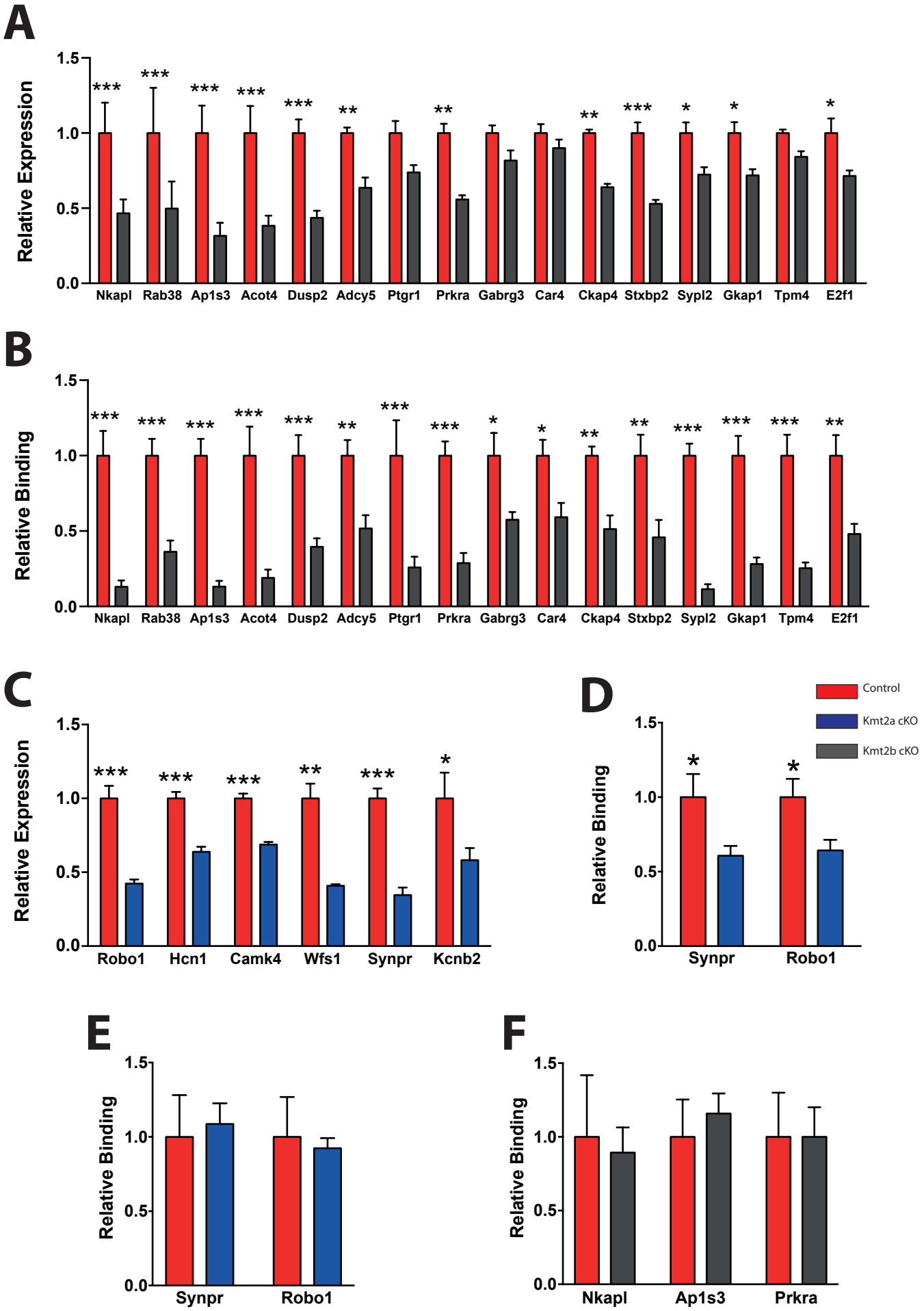

Figure S5, related to Figure 3: (A) Expression results from the current RNA-Seq for the genes previously shown to be downregulated and have decreased H3K4me3 at promoters in Kmt2b cKO mice (Kerimoglu et al., 2013). (B) H3K4me3 binding results from the current ChIP-Seq for the genes previously shown to be downregulated and have decreased H3K4me3 at promoters in Kmt2b cKO mice (Kerimoglu et al., 2013). (C) qPCR confirmation of a selection of downregulated genes in Kmt2a cKO mice compared to controls (control: n=5, Kmt2a cKO: n=6). (D) ChIP-qPCR confirmation of H3K4me3 binding at a selection of promoters in Kmt2a cKO mice compared to controls in an independent batch (control: n=5, Kmt2a cKO: n=4) (E-F) ChIP-qPCR for H3 binding at a selection of promoters with decreased H3K4me3 levels in Kmt2a cKO (control: n=4, Kmt2a cKO: n=3) (E) and Kmt2b cKO (control: n=4, Kmt2a cKO: n=3) (F) mice (*** $p < 0.001$, ** $p < 0.01$, * $p < 0.05$).

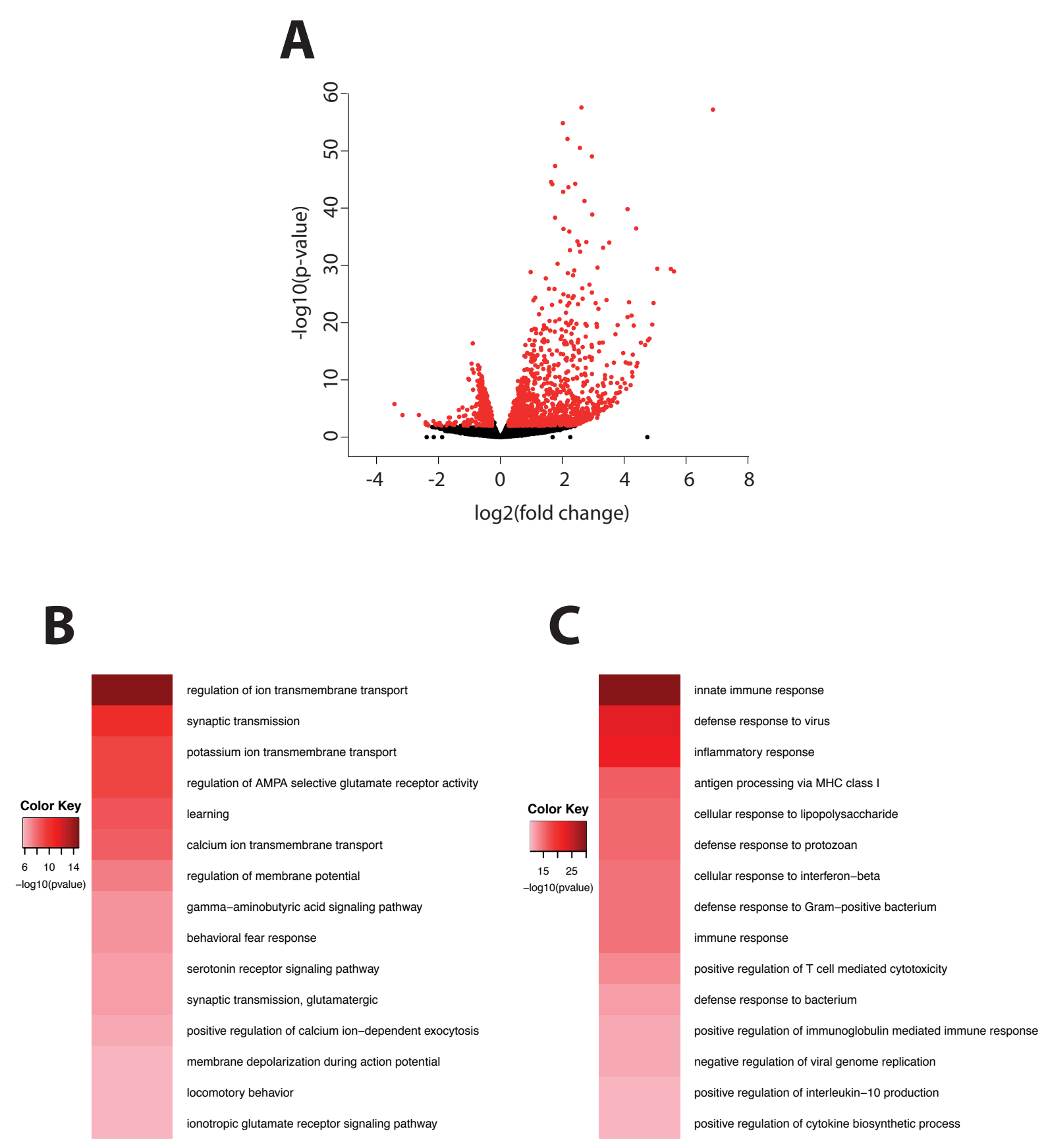

Figure S6, related to Figure 5: (A) Volcano plot depicting the differential H3K4me3 binding in hippocampus of CK-p25 mice compared to control littermates (red: FDR < 0.1 & |fold change| > 1.2). (B) Promoters with decreased H3K4me3 in CK-p25 mice largely belong to genes involved in learning & memory and synaptic plasticity-related biological processes. (C) Promoters with increased H3K4me3 in CK-p25 mice largely belong to genes involved in immune response and inflammation-related biological processes.